coatings

MDPI

Article

Cattaneo-Christov Heat Flux Model for Second Grade Nanofluid Flow with Hall Effect through Entropy Generation over Stretchable Rotating Disk

Muhammad Wakeel Ahmad [1], Luthais B. McCash [2,*], Zahir Shah [3,*] and Rashid Nawaz [1]

[1] Department of Mathematics, Abdul Wali Khan University, Mardan 23200, KPK, Pakistan; wakeel.maths@yahoo.com (M.W.A.); rashid_uop@yahoo.com (R.N.)
[2] Department of Mathematics, College of Science and Engineering, University of Leicester, University Road, Leicester LE1 7RH, UK
[3] Center of Excellence in Theoretical and Computational Science (TaCS-CoE), SCL 802 Fixed Point Laboratory, Science Laboratory Building, King Mongkut's University of Technology Thonburi (KMUTT), 126 Pracha-Uthit Road, Bang Mod, Thrung Khru, Bangkok 10140, Thailand
* Correspondence: lm460@leicester.ac.uk (L.B.M.); zahir.sha@kmutt.ac.th (Z.S.)

Received: 1 June 2020; Accepted: 22 June 2020; Published: 28 June 2020

Abstract: The second grade nanofluid flow with Cattaneo-Christov heat flux model by a stretching disk is examined in this paper. The nanofluid flow is characterized with Hall current, Brownian motion and thermophoresis influences. Entropy optimization with nonlinear thermal radiation, Joule heating and heat absorption/generation is also presented. The convergence of an analytical approach (HAM) is shown. Variation in the nanofluid flow profiles (velocities, thermal, concentration, total entropy, Bejan number) via influential parameters and number are also presented. Radial velocity, axial velocity and total entropy are enhanced with the Weissenberg number. Axial velocity, tangential velocity and Bejan number are heightened with the Hall parameter. The total entropy profile is enhanced with the Brinkman number, diffusion parameter, magnetic parameter and temperature difference. The Bejan number profile is heightened with the diffusion parameter and temperature difference. Arithmetical values of physical quantities are illustrated in Tables.

Keywords: entropy; second grade nanofluid; Cattaneo-Christov heat flux model; nanofluid; nonlinear thermal radiation; Joule heating

1. Introduction

The enhancement of heat transfer utilizing nanofluids, specifically in solar collectors, has been gaining much attention among researchers. The necessity of heat transfer improvement by ordinary fluids, like ethylene glycol, water, kerosene oil, etc., cannot be achieved. The researchers have conducted many experiments in order to develop the thermal transfer rate. Erosion and blockage are the major disadvantages in the drop of higher pressure and heat transfer rates. To reduce such problems, nanofluids are introduced. The suspension of particles of size 1–100 nm in base fluids can improve the thermal conduction in nanofluids. Using nanoparticles suspension, the thermophysical properties of conventional fluids was first proposed by Choi [1]. The applications of nanofluids are energy storage, heat exchangers, chemical industry, refrigeration process, power production, etc. Choi and Eastman [1] introduced the idea of augmenting fluids thermal conductivity. The radiation influence on nanofluid flow was discussed by Farooq et al. [2]. Sajjid et al. [3] investigated the magnetohydrodynamic (MHD) Fe_3O_4 nanofluid flow with radiation effect. The thermal and mass transmission in a nanofluid flow with chemical reaction and thermal radiation influences was presented by Sreedevi et al. [4]. The flow of silver and copper based nanofluid with radiation impact was determined by Qayyum et al. [5].

Furthermore, the same study with mixed convection and thermal radiation influences was extended by Hayat et al. [6]. The heat transfer analysis in nanofluids multi walled carbon nanotubes was discussed by Goodarzi et al. [7]. The enhancement of thermal transfer in MHD ferrofluid using different geometrical features was investigated by Goshayeshi et al. [8,9]. Other studies are cited in references [10–13]. Different materials have different properties in nature, and those materials are named viscoelastic material. Shampoo, care products, many oils and fuels, ketchup, food stuff are few examples of viscoelastic material. For describing these fluids, Jeffrey, Maxwell, Oldroyd-B, Burgers, generalized Burgers, Williamson, etc., are developed. The joule heating influence on MHD upper convected Maxwell fluid was presented by Zaidi and Mohyud-Din [14]. The MHD Maxwell fluid flow with chemical reaction was investigated by Afify and Elgazery [15]. The MHD flow of Oldroyd-B nanofluid with a heat flux model was analytically proposed by Mustafa [16]. The magnetic field impact on Williamson fluid flow in a channel was discussed by Hayat et al. [17]. The unsteady flow of Williamson fluid with radiation and heat source/sink influences was examined by Khan and Hamid [18].

Furthermore, in 1822, the mechanism of thermal transmission was suggested by Fourier's law [19]. This law leads us to the argument that the medium under consideration is immediately identifying the initial temperature. To resolve this problem, a thermal relaxation time to Fourier's law has been added by Cattaneo [20]. This term explains the required time of the medium to transmit heat to its bordering particles. Further, Christov [21] improved this model. The new model is named the heat flux model of Cattaneo-Christov (C-C). Using the C-C model, Hayat et al. [22] studied the fluid flow with homogeneous-heterogeneous reactions. The thermal transfer in an upper convected Maxwell fluid flow with C-C model was invested by Mustafa [23]. Tibullo et al. [24] presented the C-C model of heat flux, which is applicable to incompressible fluids. Han et al. [25] analyzed the couple flow of viscoelastic fluid with C-C model. Khan et al. [26] investigated the viscoelastic fluid flow over a stretching surface with a C-C model.

The consequence of Hall current on nanofluid flow has not been studied in the above mentioned literature. The modern tendency of research is in the direction of low density and strong magnetic field, due to its frequent applications like nuclear fusion, space flight, refrigeration coils, Hall accelerators, magnetohydrodynamic (MHD) generators, electric transformers, etc. The situation when the magnetic field is very strong with low density leads to conductivity reduction normal to the magnetic field. This refers to an induced current, which is called the Hall current. Under different flow configurations, numerous research works have been found. Raptis and Ram [27] examined the electrically conducting rotatory fluid flow with the Hall current. Unsteady hydrodynamic flow over a porous plate with the Hall current was inspected by Das et al. [28]. The unsteady MHD Couette flow through a rotating system with Hall and ion-slip currents combined influences was probed by Jha and Apere [29]. Aurangzeeb et al. [30] investigated the mixed convection flow with chemical reaction, heat generation and the Hall current. The convective heat transmission flow with Hall and ion-slip currents with slip conditions was determined by Ferdows et al. [31]. The numerical investigation of MHD viscous flow with Hall influence was presented by Beg et al. [32]. The MHD viscoelastic flow of fluid with hall current and convective conditions was analyzed by Kumar and Chand [33].

Entropy is the irreversibility process in a system. The heat transmission is associated with the least possible change of entropy in thermodynamics processes. Entropy generation minimization (EGM) is developed to improve the machines' ability. Spin moment, kinetic energy, vibration and internal-molecular friction are some applications of EGM. Such types of energy loss cannot be recovered deprived of additional work. That is why the measure of irreversibility process through mass and heat transfers is called entropy. The EGM process is used by investigators in many systems, like gas turbines, cooling by evaporation, natural convection, fuel cells, etc. Li and Faghri [34] investigated the EGM on high concentration direct methanol fuel cell. Hayat et al. [35] observed the EGM for peristaltic flow in a rotating frame. Nouri et al. [36] analyzed the EGM in a nanofluid flow inside a channel with a heat source. Dalir et al. [37] presented the EGM in MHD Jeffrey nanofluid over a stretching sheet.

Khan et al. [38] investigated the EGM in MHD flow of nanomaterial with binary chemical reaction and Arrhenius activation energy. The EGM in a nanomaterial mixed convective flow with slip condition was presented by Khan et al. [39]. Hayat et al. [40] presented the EGM in a second grade fluid with thermal radiation influence.

Previous studies of fluid flow over stretchable rotating disk utilizing nanofluids have not been able to consider the impacts of Cattaneo-Christov heat flux, Brownian motion and thermophoresis distribution. This paper reports on a study which considers the implications of Hall effect, Brownian motion and thermophoresis distribution on the second grade nanofluid flow with the Cattaneo-Christov heat flux model, with entropy optimization over a stretching disk. The aim of this paper is to explore a relationship between nanofluid heat transfer rate, entropy, Bejan number, Brownian motion, thermophoresis distribution and Hall effect.

2. Problem Modeling

The second grade nanofluid flow by stretchable rotating disk is assumed. The heat model of C-C is also taken in the nanofluid flow. The Hall current influence is considered in this nanofluid flow. Furthermore, EGM is considered with heat generation/absorption, Joule heating and non-linear thermal radiation. At $z = 0$ the disk rotates with angular velocity α_1. The ambient and disk temperatures are T_∞ and T_w respectively. Similarly, the ambient and surface concentrations are C_∞ and C_w. Geometry of the fluid is displayed in Figure 1.

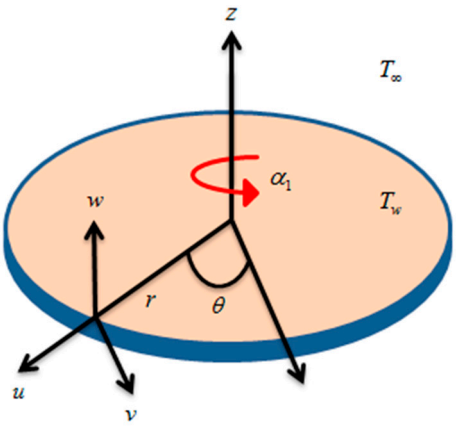

Figure 1. Fluid flow geometry.

The continuity, momentum, energy and concentration equations are taken as [40]:

$$\frac{\partial u}{\partial r} + \frac{u}{r} + \frac{\partial w}{\partial z} = 0 \tag{1}$$

$$u\frac{\partial u}{\partial r} - \frac{v^2}{r} + w\frac{\partial u}{\partial z} = \nu_f \frac{\partial^2 u}{\partial z^2} + \frac{\beta_1}{\rho_f}\left[u\frac{\partial^3 u}{\partial r \partial z^2} - \frac{1}{r}\left(\frac{\partial u}{\partial z}\right)^2 + 2w\frac{\partial u}{\partial r}\frac{\partial^2 u}{\partial z^2}\frac{\partial^3 u}{\partial z^3} + \frac{\partial v}{\partial r}\frac{\partial^2 v}{\partial z^2} + \frac{\partial w}{\partial z}\frac{\partial^2 u}{\partial z^2} + \frac{\partial v}{\partial z}\frac{\partial^2 v}{\partial r \partial z} + 3\frac{\partial u}{\partial r}\frac{\partial^2 u}{\partial r \partial z} - \frac{\partial^2 v}{\partial z^2}\frac{v}{r}\right] - \frac{\sigma_f B_0^2}{\rho_f(1+m^2)}(u + mv) \tag{2}$$

$$u\frac{\partial v}{\partial r} + \frac{uv}{r} + w\frac{\partial v}{\partial z} = \nu_f \frac{\partial^2 v}{\partial z^2} + \frac{\beta_1}{\rho_f}\left[\frac{u}{r}\frac{\partial^2 u}{\partial z^2} - 2u\frac{\partial v}{\partial z}\frac{\partial^2 u}{\partial r \partial z}\frac{\partial^3 v}{\partial r \partial z^2} + w\frac{\partial^3 v}{\partial z^3} - \frac{1}{r}\frac{\partial v}{\partial z}\frac{\partial u}{\partial z}\right] + \frac{\sigma_f B_0^2}{\rho_f(1+m^2)}(mu - v) \tag{3}$$

$$\left(\rho c_p\right)_f\left(u\frac{\partial T}{\partial r}+w\frac{\partial T}{\partial z}\right)+\gamma\left[u^2\frac{\partial^2 T}{\partial r^2}+w^2\frac{\partial^2 T}{\partial z^2}+2uw\frac{\partial^2 T}{\partial r\partial z}+\frac{\partial T}{\partial r}\left(u\frac{\partial u}{\partial r}+w\frac{\partial u}{\partial z}\right)\right.$$
$$\left.+\frac{\partial T}{\partial z}\left(u\frac{\partial w}{\partial r}+w\frac{\partial w}{\partial z}\right)\right]=k_f\frac{\partial^2 T}{\partial z^2}+Q(T-T_\infty)+\frac{\sigma_f B_0^2}{(1+m^2)}\left(u^2+v^2\right)- \quad (4)$$
$$\frac{16\sigma^*}{3k^*}\left[T^3\frac{\partial^2 T}{\partial z^2}+3T^2\left(\frac{\partial T}{\partial z}\right)^2\right]+\left(\rho c_p\right)_s\left[\frac{D_T}{T_\infty}\left(\frac{\partial T}{\partial z}\right)^2+D_B\left(\frac{\partial T}{\partial z}\frac{\partial C}{\partial z}\right)\right]$$

$$u\frac{\partial C}{\partial r}+w\frac{\partial C}{\partial z}=D_B\frac{\partial^2 C}{\partial z^2}+\frac{D_T}{T_\infty}\frac{\partial^2 T}{\partial z^2} \quad (5)$$

with

$$u=ra,\ v=r\alpha_1,\ w=0,\ T=T_w,\ C=C_w,\ \text{at}\ z=0,$$
$$u=v=0,\ T\to T_\infty,\ C\to C_\infty\ \text{when}\ z\to\infty \quad (6)$$

where u, v and w are the components of velocity in r, θ and z directions, respectively, ν_f is the kinematic viscosity, β_1 is the material parameter, k_f is the thermal conductivity, ϱ_f is the density, cp is the specific heat, Q is the heat absorption/generation, σ_f is the electrical conductivity, $(\varrho cp)_f$ is the heat capacitance, D_T is the thermophoretic diffusion coefficient and D_B is the Brownian diffusion coefficient.

Similarity transformations are defined as [40]

$$u=r\alpha_1 f'(\zeta),\ v=r\alpha_1 g(\zeta),\ w=-2h\alpha_1 f(\zeta),\ \theta=\frac{T-T_\infty}{T_w-T_\infty},\ \phi=\frac{C-C_\infty}{C_w-C_\infty},\ \zeta=\frac{z}{h} \quad (7)$$

The dimensionless forms of the leading equations are

$$f'''+\mathrm{Re}We\left(2f''^2+g'^2-2ff''''+f'f'''\right)-\mathrm{Re}\left(f'^2-2ff''-g^2\right)-\frac{M}{(1+m^2)}(f'+mg)=0 \quad (8)$$

$$g''+\mathrm{Re}We(2f'g''-2fg'''-3f''g')-\mathrm{Re}(2f'g-2fg')+\frac{M}{(1+m^2)}(mf'-g)=0 \quad (9)$$

$$\theta''+2\mathrm{Re}\mathrm{Pr}f\theta'+\mathrm{Re}\mathrm{Pr}q\theta+Nb\mathrm{Pr}\theta'\phi'+Nt\mathrm{Pr}\theta'^2-4\lambda\mathrm{Pr}\mathrm{Re}\left(f^2\theta''+ff'\theta'\right)$$
$$+Rd\left[3(\theta_w-1)\left(\theta'^2+\theta^2\theta'^2(\theta_w-1)^2+2\theta\theta'^2(\theta_w-1)\right)+\theta''+\theta^3\theta''(\theta_w-1)^3\right. \quad (10)$$
$$\left.+3(\theta_w-1)\theta\theta''+3(\theta_w-1)^2\theta^2\theta''\right]+\frac{M\mathrm{Pr}Ec}{(1+m^2)}\left(f'^2+g^2\right)=0$$

$$\phi''+2\mathrm{Re}Scf\phi'+\frac{Nt}{Nb}\theta''=0 \quad (11)$$

with

$$f(0)=0,\ f'(0)=A,\ f'(\infty)=0,\ g(0)=1,$$
$$g(\infty)=0,\ \theta(0)=1,\ \theta(\infty)=0,\ \phi(0)=1,\ \phi(\infty)=0 \quad (12)$$

where $We=\beta_1/\varrho h^2$ is the Weissenberg number, $\mathrm{Re}=\alpha_1 h^2/\nu_f$ is the Reynolds number, $A=a/\alpha_1$ is the stretching parameter, $\mathrm{Pr}=(\varrho cp)\nu_f/k_f$ is the Prandtl number, $q=Q/\varrho cp\alpha_1$ is the heat absorption/generation parameter, $Nb=\tau D_B(C_w-C_\infty)/\nu$ Brownian motion parameter, $Nt=\tau D_B(T_w-T_\infty)/T_\infty\nu$ thermophoresis parameter, $M=\sigma {B_0}^2/\alpha_1\varrho$ magnetic parameter, $Sc=\nu/D_B$ Schmidt number, $\theta_w=T_w/T_\infty$ temperature difference, $Ec=(r\alpha_1)^2/cp(T_w-T_\infty)$ is the Eckert number, $Rd=16\sigma^*{T_\infty}^3/3k_f k^*$ radiation parameter and $\lambda=r\alpha_1$ is the thermal relaxation parameter.

2.1. Skin Friction and Nusselt Number

Skin frictions along radial and tangential directions are

$$C_{fr}=\frac{\tau_{z\theta}}{\varrho(r\alpha_1)^2},\ C_{f\theta}=\frac{\tau_{zr}}{\varrho(r\alpha_1)^2} \quad (13)$$

in which τ_{zr} and $\tau_{z\theta}$ are called shear stresses in radial and tangential directions respectively, and are defined as

$$\begin{gathered}\tau_{zr} = \mu\left(\frac{\partial w}{\partial r} + \frac{\partial u}{\partial z}\right) + \beta_1\left[2\frac{\partial v}{\partial z}\left(\frac{\partial v}{\partial r} - \frac{v}{r}\right) + \left(\frac{\partial w}{\partial r} + \frac{\partial u}{\partial z}\right)\left(\frac{\partial u}{\partial r} + \frac{\partial w}{\partial z}\right) + \frac{\partial w}{\partial z}\frac{\partial u}{\partial z} + \right. \\ \left. \frac{\partial u}{\partial r}\frac{\partial w}{\partial r} + 3\left(\frac{\partial w}{\partial r}\frac{\partial w}{\partial z} + \frac{\partial u}{\partial z}\frac{\partial u}{\partial r}\right)\right] - \beta_1\left[\frac{\partial v}{\partial z}\left(\frac{\partial v}{\partial r} - \frac{v}{r}\right) + \left(\frac{\partial u}{\partial r} + \frac{\partial w}{\partial z}\right)\left(\frac{\partial w}{\partial r} + \frac{\partial u}{\partial z}\right)\right]\end{gathered} \tag{14}$$

$$\begin{gathered}\tau_{z\theta} = \mu\frac{\partial v}{\partial z} + \beta_1\left[w\frac{\partial^2 v}{\partial z^2} - \frac{v}{r}\frac{\partial u}{\partial z} + \frac{\partial v}{\partial z}\frac{\partial w}{\partial z} + u\frac{\partial^2 v}{\partial r \partial z} + \frac{\partial u}{\partial z}\frac{\partial v}{\partial r} + 3\frac{u}{r}\frac{\partial v}{\partial z}\right] \\ -\beta_1\left[\frac{\partial u}{\partial z}\frac{\partial v}{\partial r} + 2\frac{u}{r}\frac{\partial v}{\partial z} + 2\frac{\partial v}{\partial z}\frac{\partial w}{\partial z} - \frac{v}{r}\frac{\partial w}{\partial r} - \frac{v}{r}\frac{\partial u}{\partial z} + \frac{\partial w}{\partial r}\frac{\partial v}{\partial r}\right]\end{gathered} \tag{15}$$

Dimensionless forms are

$$\mathrm{Re}_r C_{fr} = f''(\zeta) + \mathrm{Re}We[3f'(\zeta)f''(\zeta) - 2f(\zeta)f'''(\zeta)]\Big|_{\zeta=0} \tag{16}$$

$$\mathrm{Re}_r C_{f\theta} = g'(\zeta) + \mathrm{Re}We[4f'(\zeta)g'(\zeta) - 2f(\zeta)g''(\zeta)]\Big|_{\zeta=0} \tag{17}$$

Heat transfer rate is defined as

$$Nu_x = \frac{hq_w}{k(T_w - T_\infty)} \tag{18}$$

where q_w is the wall heat flux, which is defined as

$$q_w\Big|_{z=0} = -\left(k + \frac{16\sigma^* T^3}{3k^*}\right)\frac{\partial T}{\partial z}\Big|_{z=0} \tag{19}$$

The dimensionless form is

$$Nu_x = -\left(1 + Rd\theta_w^3\right)\theta'(\zeta)\Big|_{\zeta=0} \tag{20}$$

2.2. Entropy Generation

$$\begin{gathered}S_G = \frac{k_f}{T_\infty^2}\left[1 + \frac{16\sigma^* T^3}{3k^* k_f}\right]\left(\frac{\partial T}{\partial z}\right)^2 + \frac{1}{T_\infty}\left[\mu_f\left(\left(\frac{\partial u}{\partial z}\right)^2 + \left(\frac{\partial v}{\partial z}\right)^2\right) + \beta_1\left[2\frac{\partial u}{\partial r}\left(\frac{\partial u}{\partial z}\right)^2\right.\right. \\ -\left(\frac{\partial u}{\partial z}\frac{\partial v}{\partial z}\frac{v}{r} + \frac{\partial v}{\partial r}\frac{\partial u}{\partial z}\frac{\partial v}{\partial z}\right) + u\frac{\partial u}{\partial z}\frac{\partial^2 u}{\partial r \partial z} + w\frac{\partial v}{\partial z}\frac{\partial^2 v}{\partial z^2} + \frac{\partial w}{\partial z}\left(\frac{\partial u}{\partial z}\right)^2 - \frac{\partial v}{\partial r}\left(\frac{\partial u}{\partial z}\right)^2 \\ \left.\left. + \frac{v}{r}\left(\frac{\partial u}{\partial z}\right)^2\right] + \frac{\sigma_f B_0^2}{T_\infty(1+m^2)}\left(u^2 + v^2\right) + \frac{R_D}{C_\infty}\left(\frac{\partial C}{\partial z}\right)^2 + \frac{R_D}{T_\infty}\left(\frac{\partial C}{\partial z}\frac{\partial T}{\partial z}\right)\end{gathered} \tag{21}$$

Equation (21) is reduced as

$$\begin{gathered}N_G = \gamma_1\left[1 + Rd(1 + \theta(\theta_w - 1))^3\right]\theta'^2 + Br\left(f''^2 + g'^2\right) + L\theta'\phi' + \\ WeBr\mathrm{Re}\left(f'f''^2 - 2f''gg' - 2fg'g''\right) + \frac{BrM}{(1+m^2)}\left(f'^2 + g^2\right) + L\frac{\gamma_2}{\gamma_1}\phi'^2\end{gathered} \tag{22}$$

The Bejan number is defined as

$$Be = \frac{\gamma_1\left[1 + Rd(1 + \theta(\theta_w - 1))^3\right]\theta'^2 + L\theta'\phi' + L\frac{\gamma_2}{\gamma_1}\phi'^2}{\left[\begin{array}{c}\gamma_1\left[1 + Rd(1 + \theta(\theta_w - 1))^3\right]\theta'^2 + Br\left(f''^2 + g'^2\right) + L\theta'\phi' + \\ WeBr\mathrm{Re}\left(\begin{array}{c} f'f''^2 - 2f''gg' \\ -2fg'g'' \end{array}\right) + \frac{BrM}{(1+m^2)}\left(f'^2 + g^2\right) + L\frac{\gamma_2}{\gamma_1}\phi'^2\end{array}\right]} \tag{23}$$

where $N_G = T_\infty h^2 S_G / k_f(T_w - T_\infty)$ is the entropy generation, $Br = \mu_f(r\alpha_1)^2/k_f(T_w - T_\infty)$ is the Brinkman number, $L = R_D(C_w - C_\infty)/k_f$ is the diffusion parameter, $\gamma_1 = (T_w - T_\infty)/T_\infty$ and $\gamma_2 = (C_w - C_\infty)/C_\infty$ are the temperature and concentration ratios, respectively.

3. HAM Solution

Linear operators are

$$L_f[f] = f''' - f',\ L_g[g] = g'' - g,\ L_\theta[\theta] = \theta'' - \theta,\ L_\phi[\phi] = \phi'' - \phi \tag{24}$$

Initial guesses are taken as

$$f_0[\zeta] = A\left[1 - e^{-\zeta}\right],\ g_0[\zeta] = \theta_0[\zeta] = \phi_0[\zeta] = e^{-\zeta} \tag{25}$$

with

$$\begin{gathered} L_f[f]\left[p_1 + p_2 e^{-\zeta} + p_3 e^{\zeta}\right] = 0,\ L_g[g]\left[p_4 e^{-\zeta} + p_5 e^{\zeta}\right] = 0, \\ L_\theta[\theta]\left[p_6 e^{-\zeta} + p_7 e^{\zeta}\right] = 0,\ L_\phi[\phi]\left[p_8 e^{-\zeta} + p_9 e^{\zeta}\right] = 0 \end{gathered} \tag{26}$$

where $P_1, P_2, P_3 \ldots, P_9$ are called constants.

Convergence Investigation

By using the auxiliary parameters $\hbar_f$, $\hbar_g$, $\hbar_\theta$ and $\hbar_\phi$, we analyzed the convergence regions for $f'(\zeta)$, $g(\zeta)$ and $\theta(\zeta)$ of the modeled system of equations. At the 25th deformation order, the $\hbar-$ curves are presented here (see Figure 2). Convergence regions for $f''(0)$, $g'(0)$, $\theta'(0)$ and $\varphi'(0)$ are $-0.06 \le \hbar_f \le 0.01$, $-0.08 \le \hbar_g \le 0.03$, $-0.11 \le \hbar_\theta \le 0.05$ and $-0.11 \le \hbar_\phi \le 0.05$, respectively.

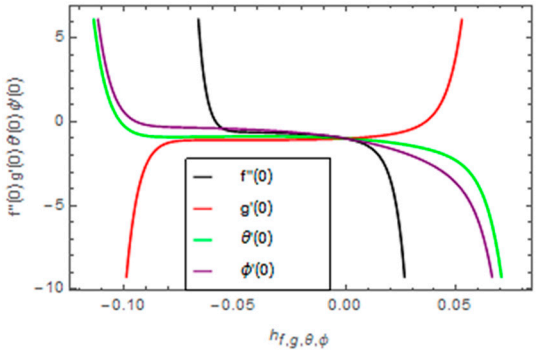

Figure 2. $\hbar-$curves for $f''(0)$, $g'(0)$, $\theta'(0)$ and $\varphi'(0)$.

4. Results and Discussion

Variation in the second grade nanofluid flow due to influential variables on $f'(\zeta)$, $g(\zeta)$, $\theta(\zeta)$, $\varphi(\zeta)$, $N_G(\zeta)$ and $Be(\zeta)$ are illustrated in Figures 3–29. The parameters are taken fixed as Re = 0.9, We = 0.3, Nb = Nt = 0.3, Ec = 0.4, q = 0.7, θ_w = 0.2, Rd = 0.5, M = 0.5, m = 0.5, Sc = 1.0 and λ = 0.1.

4.1. Velocities, Temperature and Concentration Fields

Figures 3–5 exemplify the variation in velocity profiles due to the Reynolds number. Greater Reynolds number reduces the velocity profiles in axial, radial and tangential directions. The Reynolds number is associated with the inertial forces of the fluid flow. The greater the Reynolds number, the stronger the inertial forces that reduce the motion of the fluid flow. Figures 6–8 depict the change in $f'(\zeta)$, $g(\zeta)$ and $\theta(\zeta)$ for greater m. The last terms in the principle equations of the velocity function leads us to a smaller conductivity of the fluid flow via increasing m. So, due to less conductivity, the damping force in fluid flow produces which intensifies the velocity components $f'(\zeta)$ and $g(\zeta)$. These phenomena reduce the thermal field of the fluid flow. Figures 9 and 10 illustrate the change in velocity components via the Weissenberg number. Greater values of the Weissenberg number heighten the velocity components. Increasing the Weissenberg number reduces the fluid flow viscosity. As the viscosity of the fluid is reduced, the motion of the fluid particles increase. Thus, the velocity

components escalate with a greater Weissenberg number. Figures 11–13 illustrate the change in $f'(\zeta)$, $g(\zeta)$ and $\theta(\zeta)$ via the magnetic field parameter. A higher magnetic parameter reduces the velocity components, while a reverse impact of the magnetic parameter on the thermal field is observed. The heightening magnetic field produces higher resistive force to the flow of fluid, which drops the motion of the fluid flow. Thus, the velocity components decline. On the other hand, the higher resistive force increases the electrons collision, which produces more heat to fluid flow. Therefore, the thermal field rises with the higher values of magnetic parameter. Figures 14 and 15 exhibit the change in velocity components ($f(\zeta)$, $g(\zeta)$) via a stretching parameter. The momentum boundary layer escalates with higher values of stretching parameter and, consequently, the velocity profile $f(\zeta)$ heightens. On the other hand, the velocity profile $g(\zeta)$ declines with a higher stretching parameter. This influence is due to the fact that the higher values of stretching parameter reduce the angular velocity of the fluid flow. Figure 16 displays the change in thermal field via Brownian motion and thermophoresis parameters. The rising values of Brownian motion and thermophoresis parameters intensify the thermal field. The rising thermophoretic force pushes the fluid particles to move form heated to cold regions and, consequently, the temperature field increases. A similar impact is also depicted against the Brownian motion parameter. Figure 17 shows the change in thermal profile via thermal relaxation parameter. Higher values of relaxation parameter decline the temperature profile. With higher values of thermal relaxation parameter, the material particles need more potential to transmit energy to its surrounding particles. Additionally, this behavior is less for the C-C model as compared to Fourier's law. Figure 18 illustrates the change in thermal field via temperature difference parameter. An escalating conduct is detected in thermal field by heightening the temperature difference parameter. By increasing the temperature difference parameter, the temperature at the wall increases, and then the ambient temperature also increases. Consequently, the temperature field heightens. Figure 19 clarifies the change in thermal field via heat generation/absorption parameter. Clearly, the increasing heat parameter increases the temperature profile. The heat generation/absorption parameter acts like a heat generator. The increasing generation/absorption increases the thermal field of the fluid flow. Figure 20 indicates the change in thermal profile via the Prandtl number. A declining impact is detected via increasing Prandtl number. Figure 21 indicates the variation in concentration field via thermophoresis parameter. As the increasing thermophoresis parameter increases the thermal field (see Figure 16), consequently, the concentration of the fluid flow also increases. The opposite impact of Brownian motion parameter is depicted against the concentration profile (see Figure 22). The change in concentration field via the Schmidt number is displayed in Figure 23. A declining impact is observed here. The concentration distribution in inversely related with the Schmidt number. The intensifying estimations of the Schmidt number reduce the thickness of the boundary layer flow. The concentration distribution therefore declines.

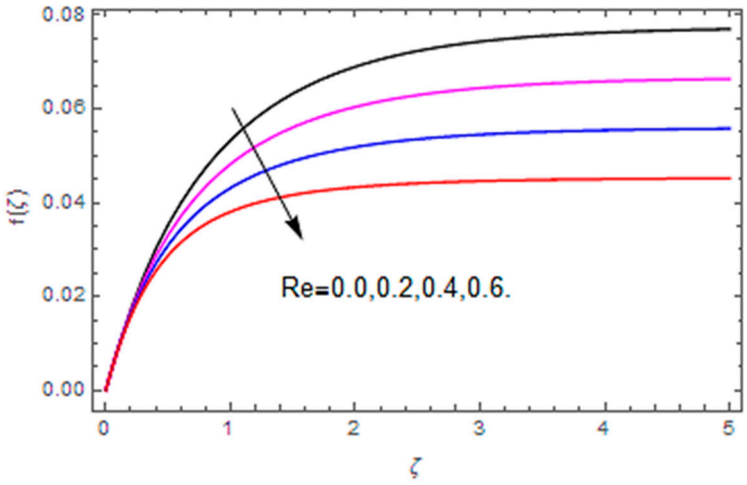

Figure 3. Re on $f(\zeta)$.

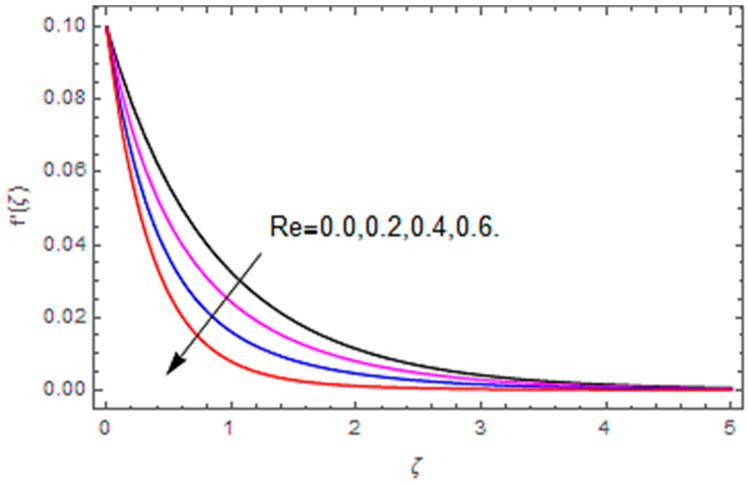

Figure 4. Re on $f'(\zeta)$.

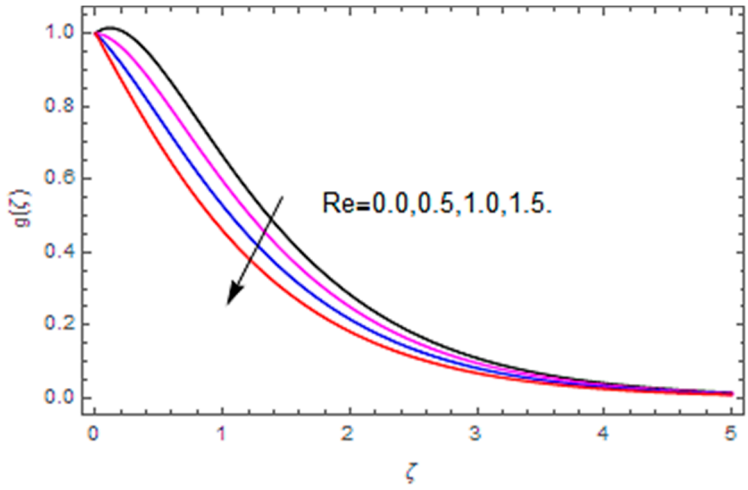

Figure 5. Re on $g(\zeta)$.

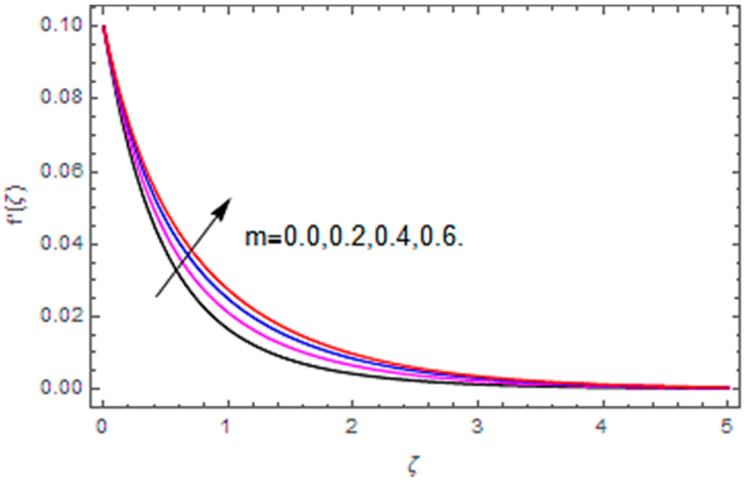

Figure 6. m on $f'(\zeta)$.

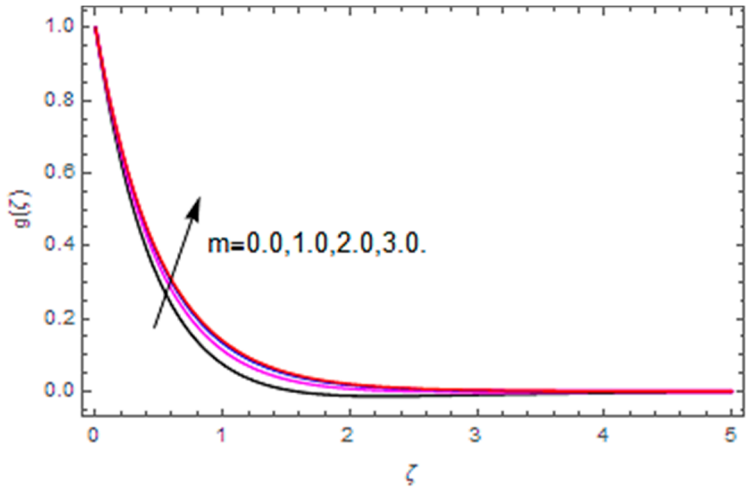

Figure 7. m on $g(\zeta)$.

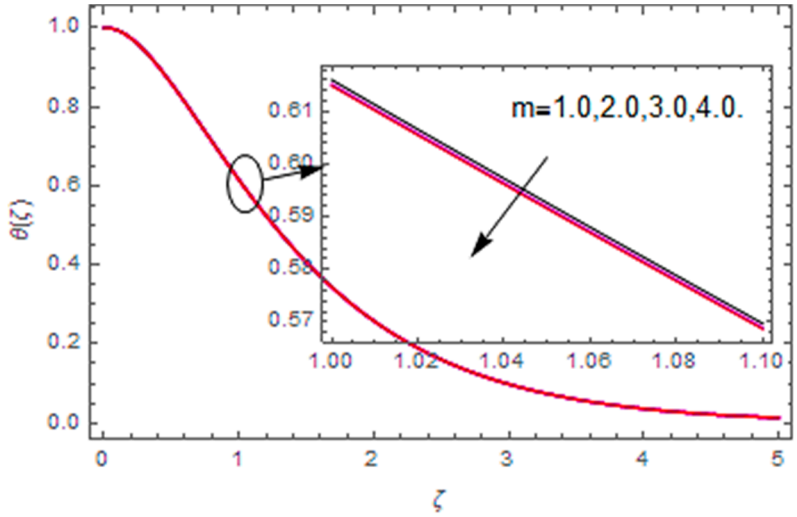

Figure 8. m on $\theta(\zeta)$.

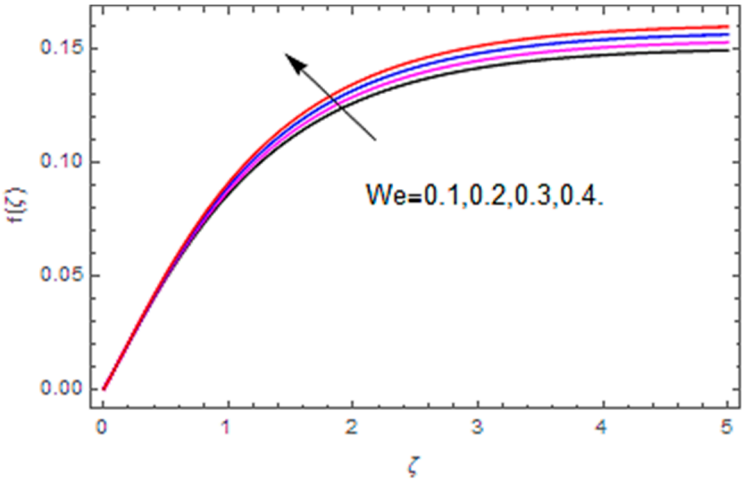

Figure 9. We on $f(\zeta)$.

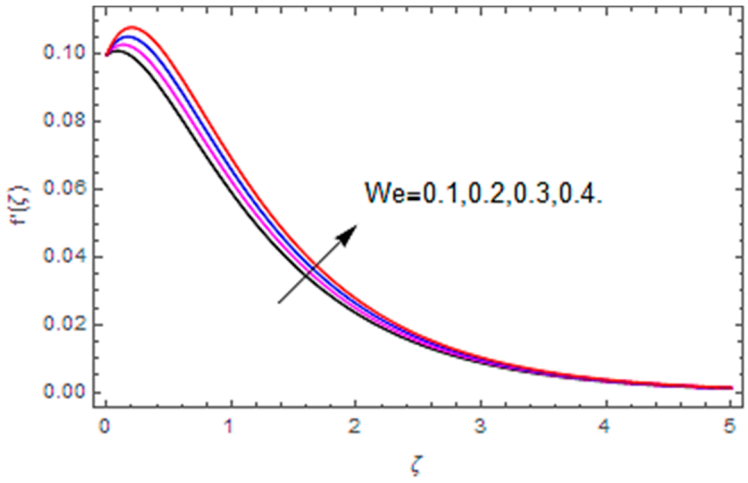

Figure 10. *We* on $f'(\zeta)$.

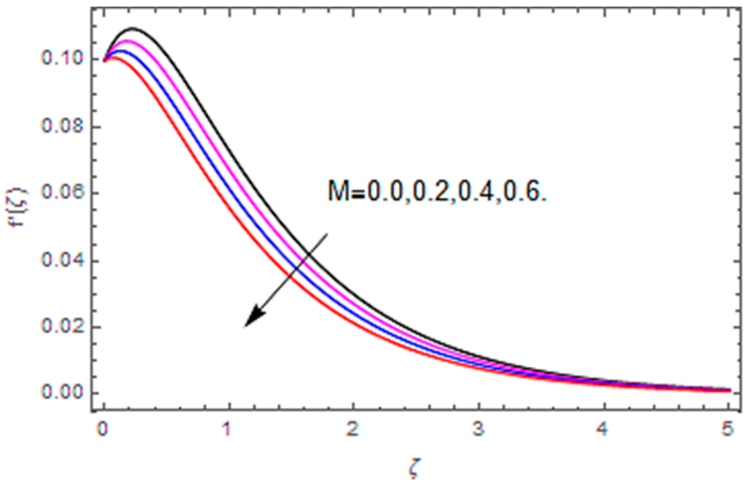

Figure 11. *M* on $f'(\zeta)$.

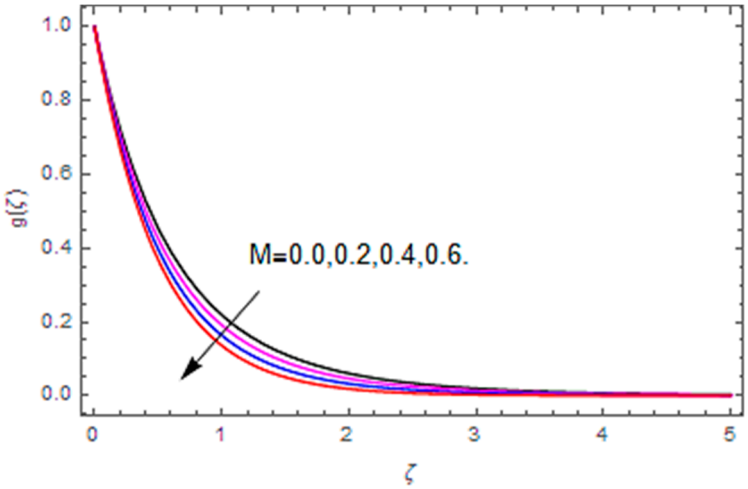

Figure 12. *M* on $g(\zeta)$.

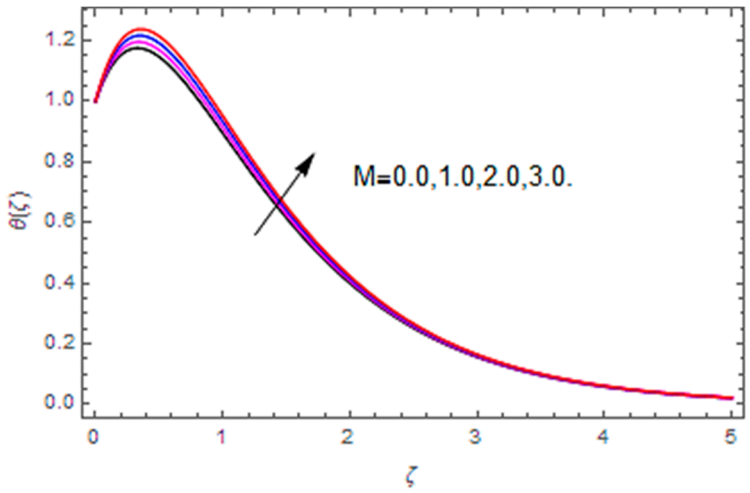

Figure 13. *M* on θ(ζ).

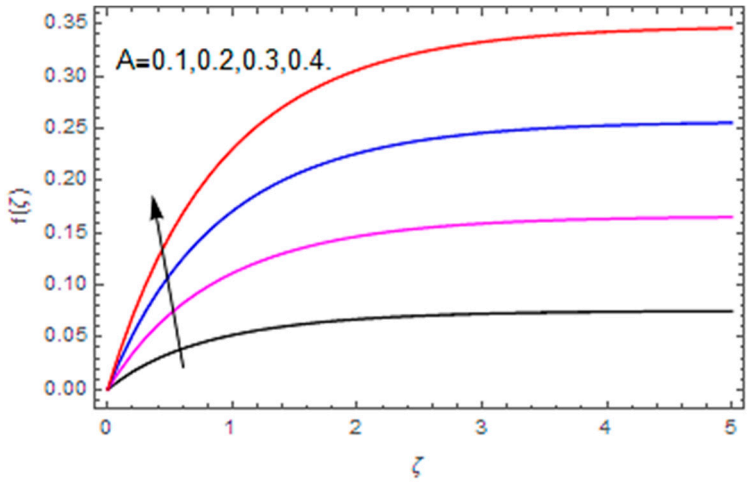

Figure 14. *A* on *f*(ζ).

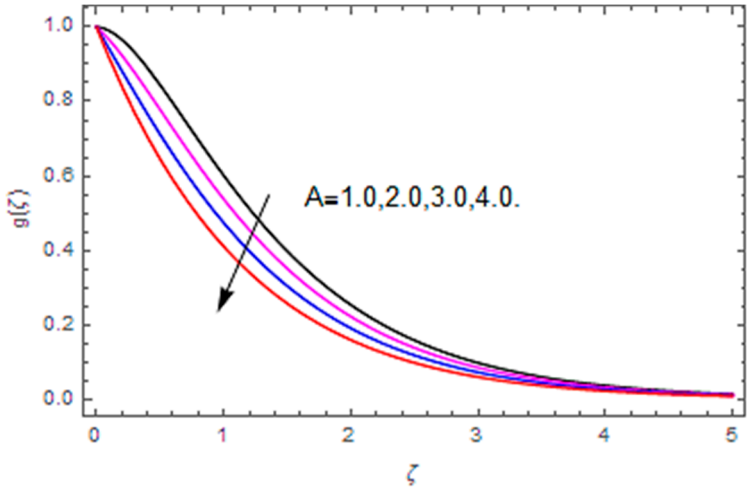

Figure 15. *A* on *g*(ζ).

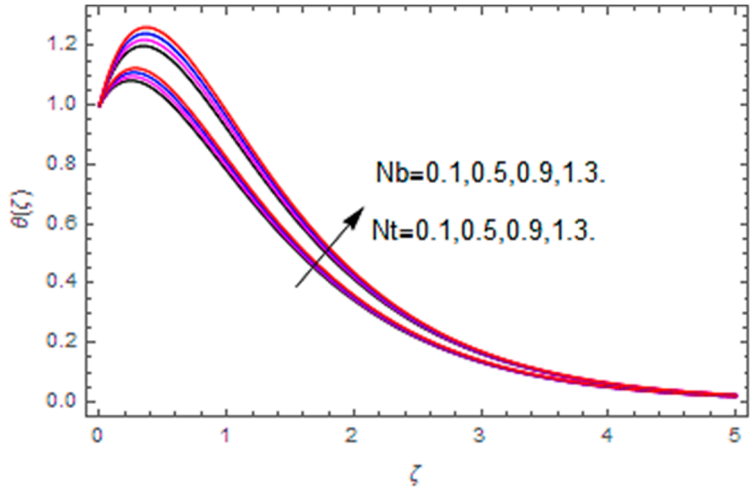

Figure 16. *Nb* and *Nt* on θ(ζ).

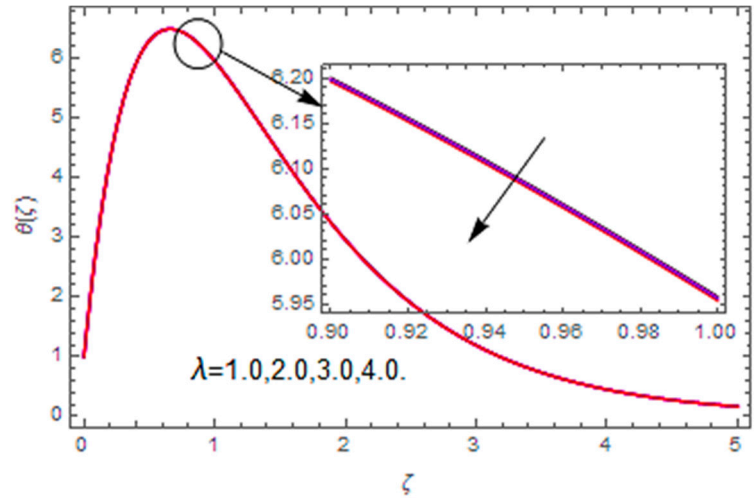

Figure 17. λ on θ(ζ).

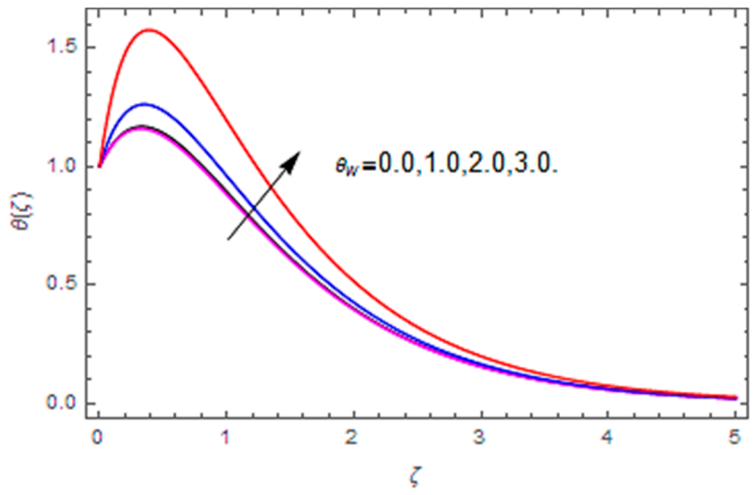

Figure 18. θ_w on θ(ζ).

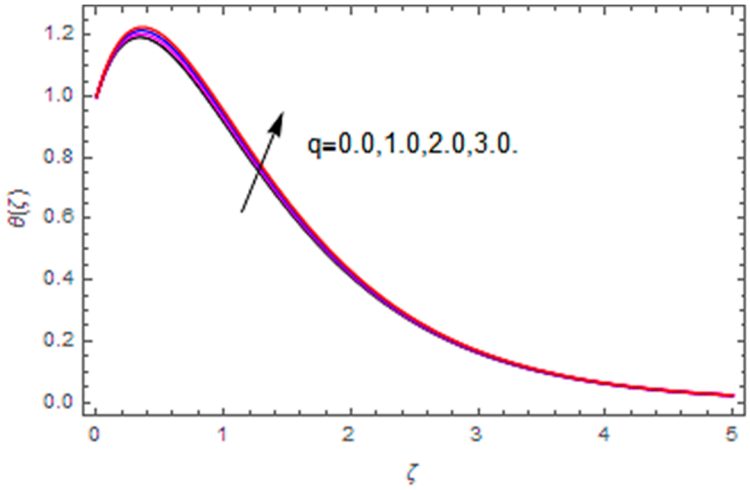

Figure 19. q on θ(ζ).

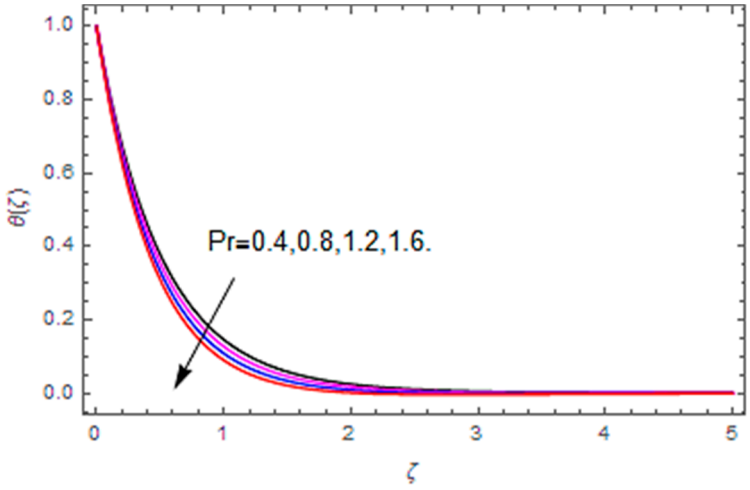

Figure 20. Pr on θ(ζ).

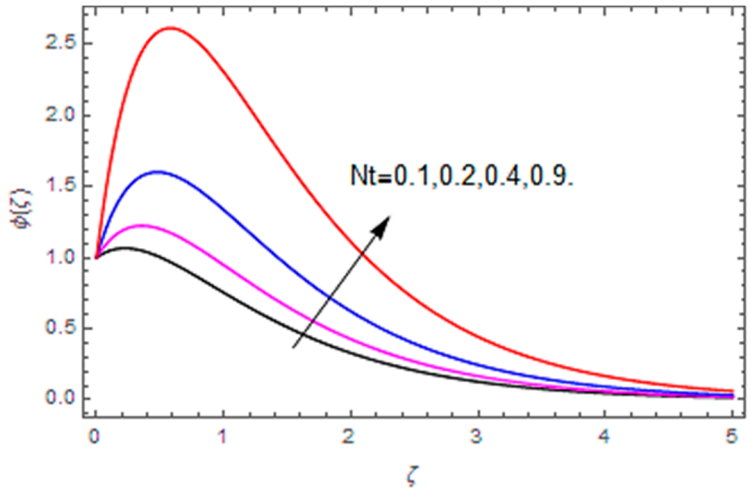

Figure 21. Nt on φ(ζ).

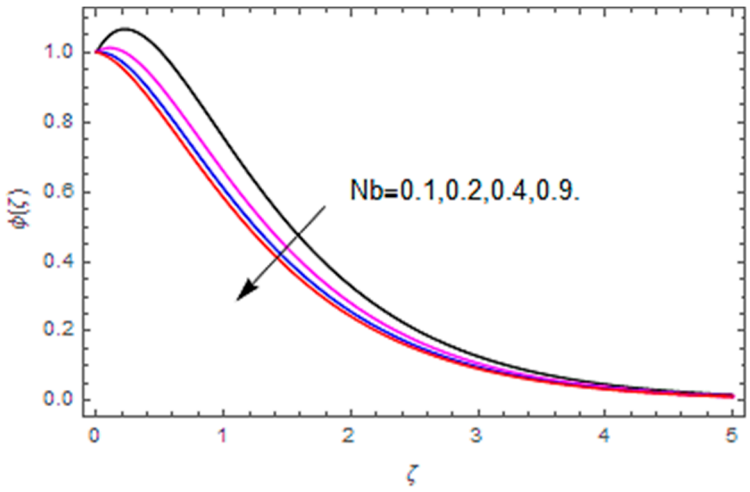

Figure 22. *Nb* on φ(ζ).

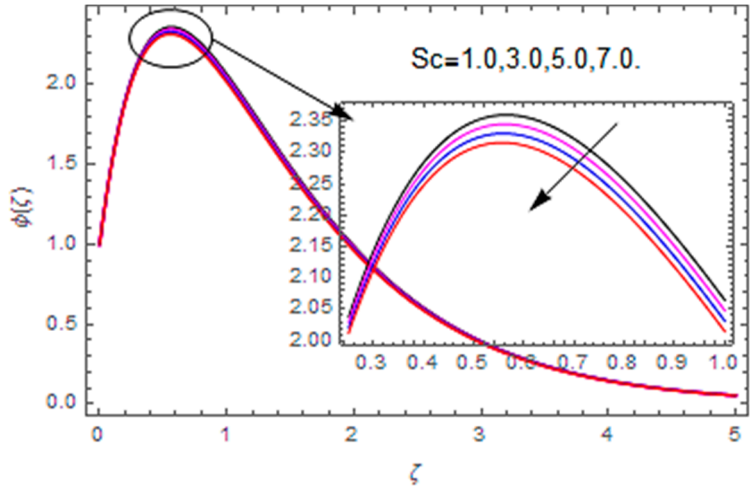

Figure 23. *Sc* on φ(ζ).

4.2. Entropy Optimization and Bejan Number

Figures 24 and 25 depict the impact of Brinkman number on the total entropy profile and the Bejan number profile, respectively. The total entropy profile escalates with a higher Brinkman number, while the opposite trend is observed on the Bejan number profile. The heat rises in the fluid moving in related region heightens with greater Brinkman number. Therefore, the total entropy profile rises with the Brinkman number, and the Bejan number declines (see Figure 25). Figures 26 and 27 illustrate the change in the total entropy profile and the Bejan number profile, via greater values of the diffusion parameter. Both total entropy and the Bejan number profiles escalate with larger values of diffusion parameter. The rising diffusion parameter increases the nanoparticle's diffusion rate. Thus, both profiles escalate with a greater diffusion parameter. Figures 28 and 29 display the change in total entropy and Bejan number profiles via the magnetic parameter. The total entropy profile escalates, while the Bejan number profile deescalates with a higher magnetic parameter. According to the Lorentz force, the total entropy of the system heightens, while the Bejan number reduces with higher magnetic parameter. So, the total entropy profile escalates, while the Bejan number profile deescalates with a higher magnetic parameter. Figures 30 and 31 illustrate the change in total entropy and the Bejan number profiles via temperature difference parameters. Both profiles escalate with higher temperature difference parameters. Figures 32 and 33 show the change in total entropy and Bejan number profiles via the Weissenberg number. Increasing the Weissenberg number reduces the fluid flow viscosity.

This behavior escalates both total entropy and the Bejan number profiles. Figures 34 and 35 indicate the variation the total entropy and Bejan number profiles via the Hall parameter. The total entropy profile declines, while the Bejan number profile escalates with the higher Hall parameter. The Hall parameter has a direct effect on the Lorentz force term and current density of the nanofluid. Thus, the electrical conductivity of the nanofluid heightens with the higher Hall parameter and, consequently, the total entropy profile is reduced. The opposite impact of Hall parameter on the Bejan number is displayed in Figure 35.

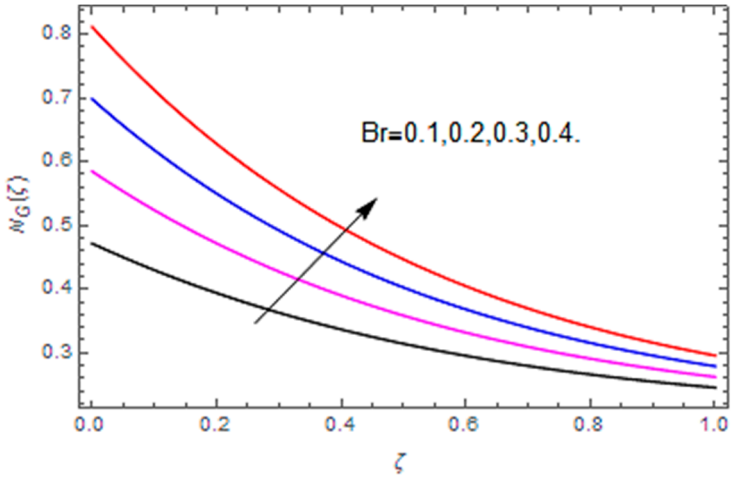

Figure 24. *Br* on $N_G(\zeta)$.

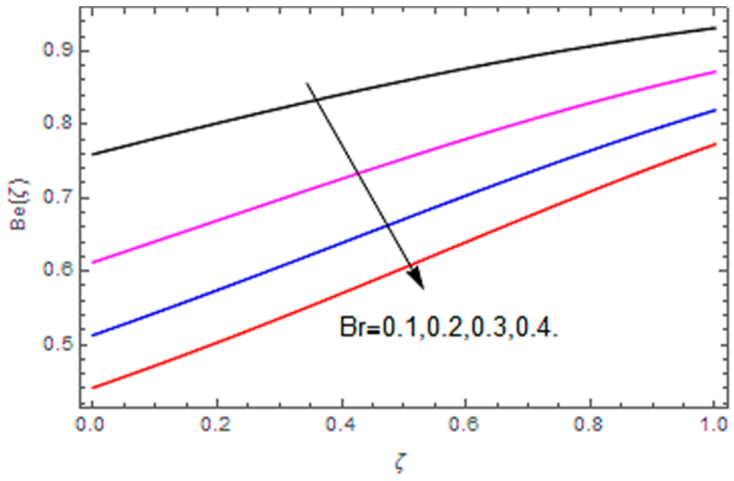

Figure 25. *Br* on $Be(\zeta)$.

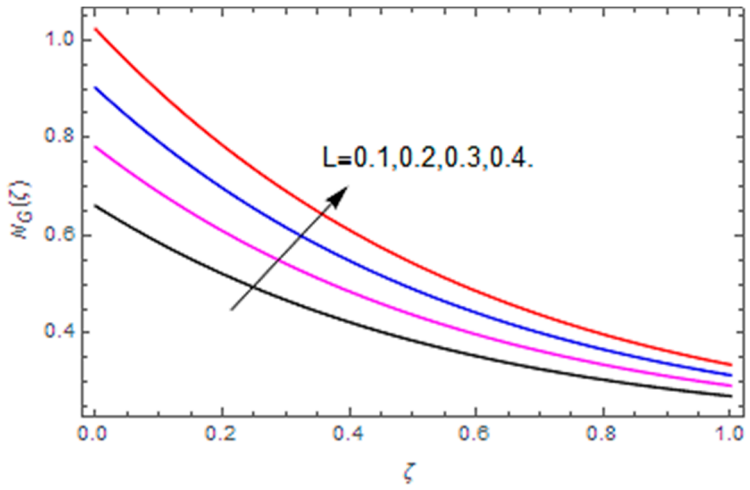

Figure 26. L on $N_G(\zeta)$.

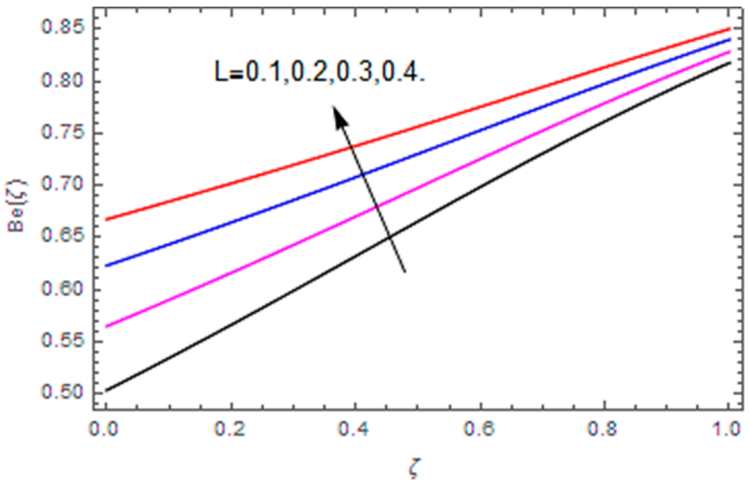

Figure 27. L on $Be(\zeta)$.

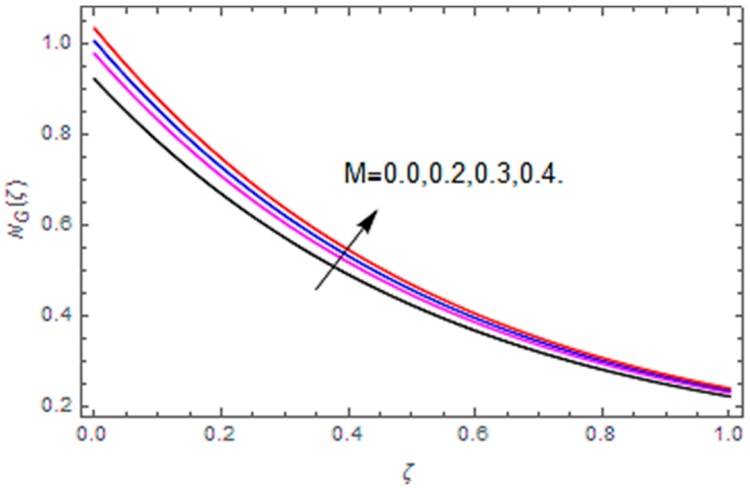

Figure 28. M on $N_G(\zeta)$.

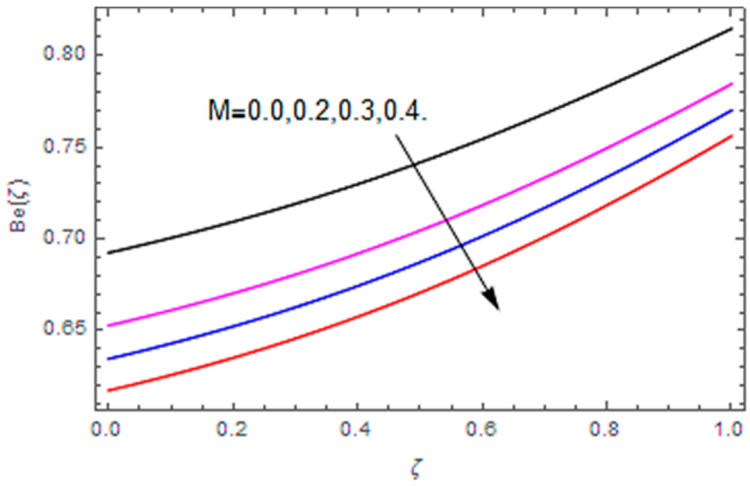

Figure 29. M on $Be(\zeta)$.

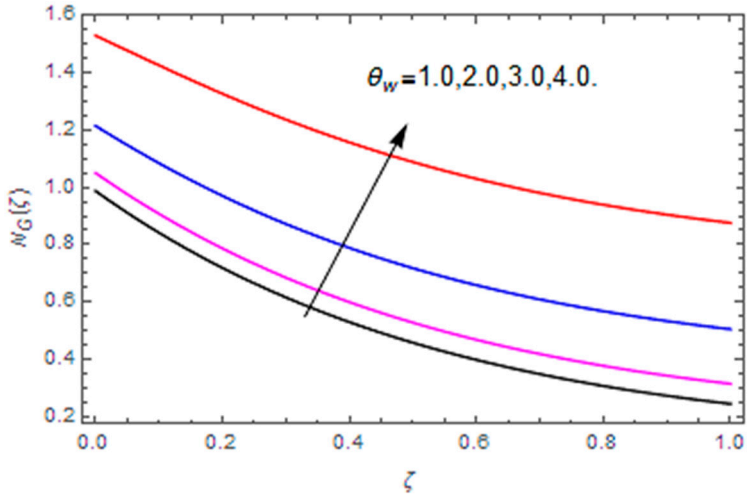

Figure 30. θ_w on $N_G(\zeta)$.

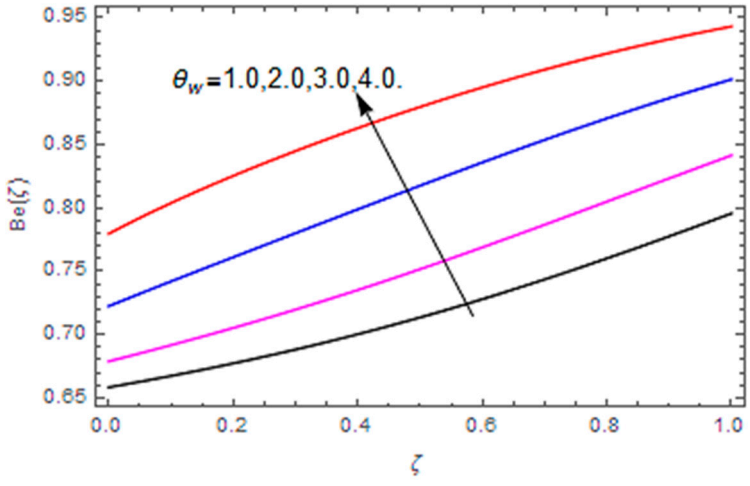

Figure 31. θ_w on $Be(\zeta)$.

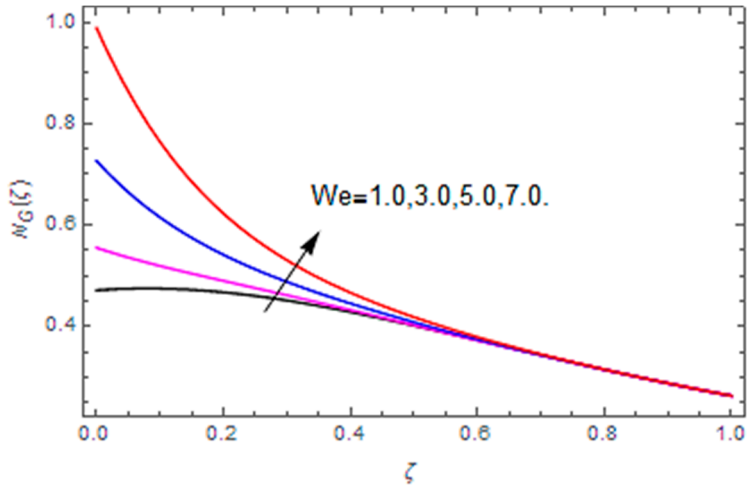

Figure 32. *We* on $N_G(\zeta)$.

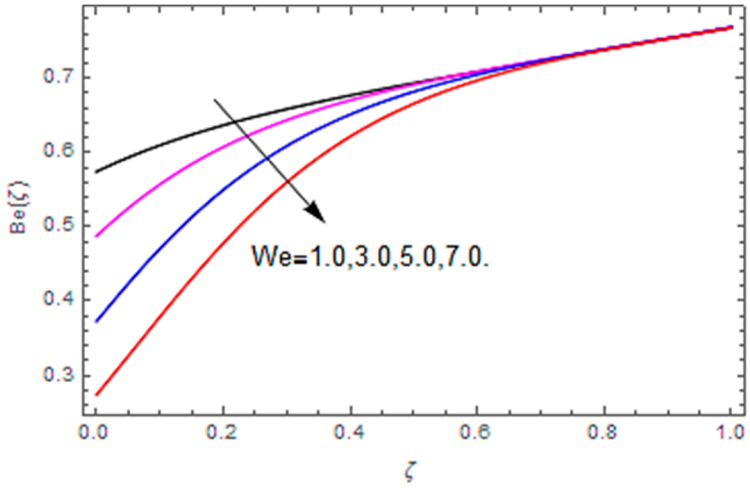

Figure 33. *We* on $Be(\zeta)$.

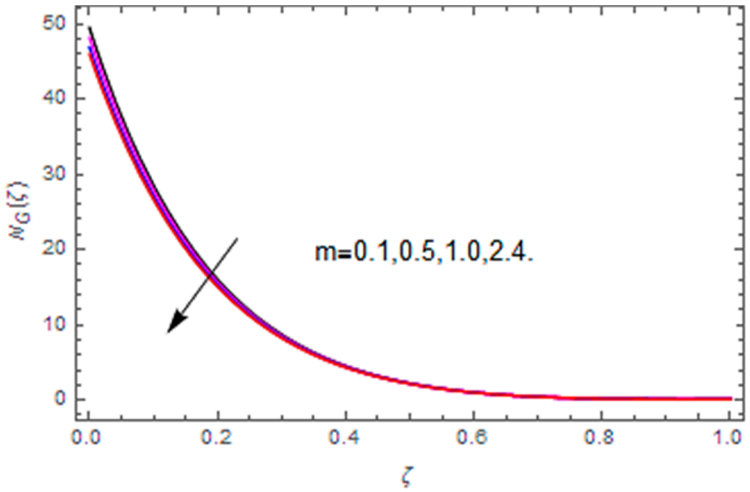

Figure 34. *m* on $N_G(\zeta)$.

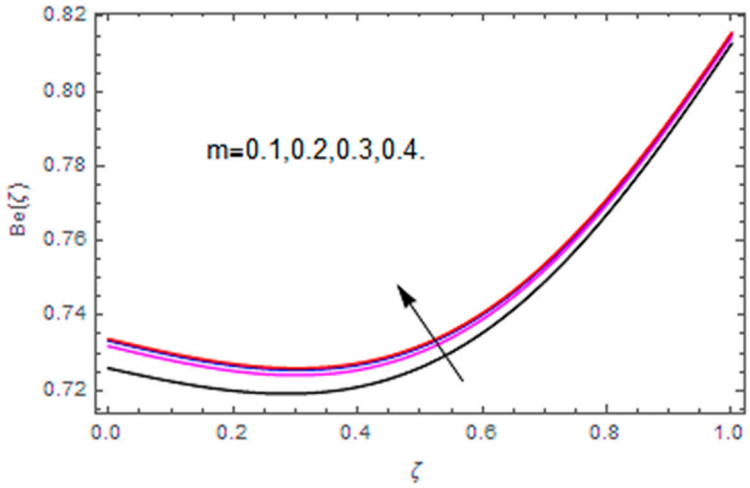

Figure 35. m on $Be(\zeta)$.

4.3. Physical Quantities

The values of skin friction along radial and tangential directions are presented in Table 1. The higher Weissenberg and Reynolds numbers increase the skin friction, while the magnetic, Hall and stretching parameters have a reducing influence on the skin friction along the radial direction. The heightening magnetic parameter escalates the skin friction while opposite trend is observed via the Weissenberg number, Reynods number, Hall parameter and stretching parameter along a tangential direction. Table 2 represents the values of Nu_x, via influential parameters and numbers. The rising values of λ, heightens Nu_x, while increasing Re, Pr, q, Nb, Nt, Ec and θ_w reducing Nu_x.

Table 1. Numerical values of skin friction along radial (Re_r, C_{fr}) and tangential (Re_θ, $C_{f\theta}$) directions.

We	Re	*M*	*m*	*A*	$\mathrm{Re}_r C_{fr}$	$\mathrm{Re}_\theta C_{f\theta}$
0.2	0.5	0.3	0.2	0.1	0.076871	−0.578141
0.3	–	–	–	–	0.109318	−0.601784
0.4	–	–	–	–	0.126191	−0.613634
–	0.0	–	–	–	−0.073910	−0.529679
–	1.0	–	–	–	0.349447	−0.703740
–	1.5	–	–	–	0.595858	−0.800002
–	–	0.0	–	–	0.608339	−0.928553
–	–	0.2	–	–	0.600019	−0.842866
–	–	0.5	–	–	0.587538	−0.714335
–	–	–	0.3	–	0.588645	−0.726248
–	–	–	0.5	–	0.539113	−0.755780
–	–	–	0.7	–	0.521225	−0.786661
–	–	–	–	0.2	0.536944	−1.122600
–	–	–	–	0.4	0.531917	−1.973220
–	–	–	–	0.5	0.514140	−2.487880

Table 2. Numerical values of Nusselt number (Nu_x).

Re	Pr	q	Nb	Nt	λ	Ec	θ_w	Nu_x
0.0	0.72	0.3	0.4	0.4	0.1	0.2	0.3	0.436148
1.0	–	–	–	–	–	–	–	0.425559
1.5	–	–	–	–	–	–	–	0.420265
–	0.4	–	–	–	–	–	–	0.502356
–	0.8	–	–	–	–	–	–	0.399743
–	1.2	–	–	–	–	–	–	0.297129
–	–	0.4	–	–	–	–	–	0.230951
–	–	0.5	–	–	–	–	–	0.164773
–	–	0.6	–	–	–	–	–	0.098594
–	–	–	0.5	–	–	–	–	0.065505
–	–	–	0.6	–	–	–	–	0.032416
–	–	–	0.7	–	–	–	–	−0.000672
–	–	–	–	0.5	–	–	–	−0.033761
–	–	–	–	0.6	–	–	–	−0.066850
–	–	–	–	0.7	–	–	–	−0.099939
–	–	–	–	–	0.3	–	–	0.111830
–	–	–	–	—	0.5	–	–	0.125066
–	–	–	–	–	0.7	–	–	0.138302
–	–	–	–	–	–	0.3	–	0.129974
–	–	–	–	–	–	0.4	–	0.121646
–	–	–	–	–	–	0.5	–	0.113318
–	–	–	–	–	–	–	1.0	0.116974
–	–	–	–	–	–	–	1.5	0.041694
–	–	–	–	–	–	–	2.0	−0.296988

5. Conclusions

The second grade nanofluid flow by a stretching disk is examined here. The nanofluid flow is characterized with Hall current, Brownian motion and thermophoresis influences. Entropy optimization with nonlinear thermal radiation, Joule heating and heat absorption/generation is also presented. Concluding remarks are mentioned below:

- Velocity along the radial direction is enhanced with the Weissenberg number and stretching parameter, however, the conflicting influence is observed via the Reynolds number.
- Velocity along the axial direction is heightened with the Hall parameter and Weissenberg number, while it is decreased with the magnetic parameter and the Reynolds number.
- Velocity along the tangential direction is escalated with the Hall parameter, while it decays with the magnetic parameter, Reynolds number and stretching parameter.
- The temperature profile is increased with the magnetic parameter, Brownian motion parameter, thermophoresis parameter, temperature difference and heat generation/absorption parameter, whereas it is reduced with the Hall parameter, thermal relaxation parameter and Prandtl number.
- The concentration profile is increased with the thermophoresis parameter, while it is reduced with the Brownian motion parameter and the Schmidt number.
- The total entropy profile is enhanced with the Brinkman number, diffusion parameter, magnetic parameter, temperature difference and Weissenberg number, while a declining influence is detected via the Hall parameter.
- The Bejan number profile is heightened with diffusion parameter, temperature difference and Hall parameter, while it is diminished with the Brinkman number, magnetic parameter and Weissenberg number.

Author Contributions: Conceptualization, Z.S. and L.B.M.; methodology, M.W.A.; software, Z.S.; validation, R.N. and Z.S.Y.; formal analysis, L.B.M.; investigation, Z.S.; resources, L.B.M.; data curation, M.W.A.; writing—original draft preparation, M.W.A and L.B.M.; writing—review and editing, Z.S. and R.N.; visualization, L.B.M.; supervision, Z.S. and R.N.; project administration, L.B.M.; funding acquisition, L.B.M. All authors have read and agreed to the published version of the manuscript.

Funding: This research received no external funding.

Acknowledgments: This research is supported by Postdoctoral Fellowship from King Mongkut's University of Technology Thonburi (KMUTT), Thailand.

Conflicts of Interest: The authors declare no conflict of interest.

References

1. Choi, S.U.; Eastman, J.A. *Enhancing Thermal Conductivity of Fluids with Nanoparticles*; No. ANL/MSD/CP-84938; CONF-951135-29; Argonne National Lab.: Cass Ave, IL, USA, 1995.
2. Farooq, M.; Khan, M.I.; Waqas, M.; Hayat, T.; Alsaedi, A.; Khan, M.I. MHD stagnation point flow of viscoelastic nanofluid with non-linear radiation effects. *J. Molecul. Liq.* **2016**, *221*, 1097–1103. [CrossRef]
3. Sajid, M.; Iqbal, S.A.; Naveed, M.; Abbas, Z. Effect of homogeneous-heterogeneous reactions and magnetohydrodynamics on Fe_3O_4 nanofluid for the Blasius flow with thermal radiations. *J. Molecul. Liq.* **2017**, *233*, 115–121. [CrossRef]
4. Sreedevi, P.; Reddy, P.S.; Chamkha, A.J. Heat and mass transfer analysis of nanofluid over linear and non-linear stretching surfaces with thermal radiation and chemical reaction. *Powder Technol.* **2017**, *315*, 194–204. [CrossRef]
5. Qayyum, S.; Khan, M.I.; Hayat, T.; Alsaedi, A. A framework for nonlinear thermal radiation and homogeneous-heterogeneous reactions flow based on silver-water and copper-water nanoparticles: A numerical model for probable error. *Results Phys.* **2017**, *7*, 1907–1914. [CrossRef]
6. Hayat, T.; Qayyum, S.; Imtiaz, M.; Alsaedi, A. Comparative study of silver and copper water nanofluids with mixed convection and nonlinear thermal radiation. *Int. J. Heat Mass Transf.* **2016**, *102*, 723–732. [CrossRef]
7. Goodarzi, M.; Amiri, A.; Goodarzi, M.S.; Safaei, M.R.; Karimipour, A.; Languri, E.M.; Dahari, M. Investigation of heat transfer and pressure drop of a counter flow corrugated plate heat exchanger using MWCNT based nanofluids. *Int. Commun. Heat Mass Transf.* **2015**, *66*, 172–179. [CrossRef]
8. Goshayeshi, H.R.; Goodarzi, M.; Safaei, M.R.; Dahari, M. Experimental study on the effect of inclination angle on heat transfer enhancement of a ferrofluid in a closed loop oscillating heat pipe under magnetic field. *Exp. Therm. Fluid Sci.* **2016**, *74*, 265–270. [CrossRef]
9. Goshayeshi, H.R.; Safaei, M.R.; Goodarzi, M.; Dahari, M. Particle size and type effects on heat transfer enhancement of Ferro-nanofluids in a pulsating heat pipe. *Powder Technol.* **2016**, *301*, 1218–1226. [CrossRef]
10. Hosseini, S.M.; Safaei, M.R.; Goodarzi, M.; Alrashed, A.A.; Nguyen, T.K. New temperature, interfacial shell dependent dimensionless model for thermal conductivity of nanofluids. *Int. J. Heat Mass Transf.* **2017**, *114*, 207–210. [CrossRef]
11. Peng, Y.; Zahedidastjerdi, A.; Abdollahi, A.; Amindoust, A.; Bahrami, M.; Karimipour, A.; Goodarzi, M. Investigation of energy performance in a U-shaped evacuated solar tube collector using oxide added nanoparticles through the emitter, absorber and transmittal environments via discrete ordinates radiation method. *J. Therm. Anal. Calorim.* **2020**, *139*, 2623–2631. [CrossRef]
12. Shamshirband, S.; Malvandi, A.; Karimipour, A.; Goodarzi, M.; Afrand, M.; Petković, D.; Dahari, M.; Mahmoodian, N. Performance investigation of micro-and nano-sized particle erosion in a 90 elbow using an ANFIS model. *Powder Technol.* **2015**, *284*, 336–343. [CrossRef]
13. Tian, Z.; Etedali, S.; Afrand, M.; Abdollahi, A.; Goodarzi, M. Experimental study of the effect of various surfactants on surface sediment and pool boiling heat transfer coefficient of silica/DI water nano-fluid. *Powder Technol.* **2019**, *356*, 391–402. [CrossRef]
14. Zaidi, Z.A.; Mohyud-Din, S.T. Effect of joule heating and MHD in the presence of convective boundary condition for upper convected Maxwell fluid through wall jet. *J. Mol. Liq.* **2017**, *230*, 230–234. [CrossRef]

15. Afify, A.A.; Elgazery, N.S. Effect of a chemical reaction on magnetohydrodynamic boundary layer flow of a Maxwell fluid over a stretching sheet with nanoparticles. *Particuology* **2016**, *29*, 154–161. [CrossRef]
16. Mustafa, M. An analytical treatment for MHD mixed convection boundary layer flow of Oldroyd-B fluid utilizing non-Fourier heat flux model. *Int. J. Heat Mass Transf.* **2017**, *113*, 1012–1020. [CrossRef]
17. Hayat, T.; Nawaz, S.; Alsaedi, A.; Rafiq, M. Influence of radial magnetic field on the peristaltic flow of Williamson fluid in a curved complaint walls channel. *Results phys.* **2017**, *7*, 982–990. [CrossRef]
18. Khan, M.; Hamid, A. Influence of non-linear thermal radiation on 2D unsteady flow of a Williamson fluid with heat source/sink. *Results phys.* **2017**, *7*, 3968–3975. [CrossRef]
19. Baron Fourier, J.B.J. Théorie Analytique de la Chaleur. In *Landmark Writings in Western Mathematics 1640–1940*; Elsevier: Amsterdam, The Netherlands, 2005.
20. Cattaneo, C. Sulla conduzione del calore. *Atti Sem. Mat. Fis. Univ. Modena* **1948**, *3*, 83–101.
21. Christov, C.I. On frame indifferent formulation of the Maxwell–Cattaneo model of finite-speed heat conduction. *Mech. Res. Commun.* **2009**, *36*, 481–486. [CrossRef]
22. Hayat, T.; Qayyum, S.; Imtiaz, M.; Alsaedi, A. Impact of Cattaneo-Christov heat flux in Jeffrey fluid flow with homogeneous-heterogeneous reactions. *PLoS ONE* **2016**, *11*, e0148662. [CrossRef]
23. Mustafa, M. Cattaneo-Christov heat flux model for rotating flow and heat transfer of upper-convected Maxwell fluid. *AIP Adv.* **2015**, *5*, 047109. [CrossRef]
24. Tibullo, V.; Zampoli, V. A uniqueness result for the Cattaneo-Christov heat conduction model applied to incompressible fluids. *Mech. Res. Commun.* **2011**, *38*, 77–99. [CrossRef]
25. Han, S.; Zheng, L.; Li, C.; Zhang, X. Coupled flow and heat transfer in viscoelastic fluid with Cattaneo-Christov heat flux model. *Appl. Math. Lett.* **2014**, *38*, 87–93. [CrossRef]
26. Ahmad Khan, J.; Mustafa, M.; Hayat, T.; Alsaedi, A. Numerical study of Cattaneo-Christov heat flux model for viscoelastic flow due to an exponentially stretching surface. *PLoS ONE* **2015**, *10*, e0137363. [CrossRef]
27. Raptis, A.; Ram, P.C. Effects of hall current and rotation. *Astrophys. Space Sci.* **1984**, *106*, 257–264. [CrossRef]
28. Das, S.; Maji, S.L.; Jana, R.N. Hall effects on unsteady hydromagnetic flow induced by a porous plate. *Int. J. Comput. Appli.* **2012**, *57*, 37–44.
29. Jha, B.K.; Apere, C.A. Combined effect of hall and ion-slip currents on unsteady MHD couette flows in a rotating system. *J. Phys. Soc. Jpn.* **2010**, *79*, 1–9.
30. Aurangzeeb, S.; Shafie, S. Effects of Soret and Dufour on unsteady MHD flow by mixed convection over a vertical surface in porous media with internal heat generation, chemical reaction and Hall current. *Can. J. Sci. Eng. Math.* **2011**, *2*, 153–162.
31. Ferdows, M.; Jahan, E.; Hamad, M.M.; Masahiro, O.T.A. Effects of Hall and ion-slip currents on free convective heat transfer flow past a vertical plate considering slip conditions. *Can. J. Sci. Eng. Math.* **2011**, *2*, 70–76.
32. Anwar Bég, O.; Sim, L.; Zueco, J.; Bhargava, R. Numerical study of magnetohydro-dynamic viscous plasma flow in rotating porous media with Hall currents and inclined magnetic field influence. *Commun. Nonlinear Sci. Numer. Simul.* **2010**, *15*, 345–359.
33. Kumar, R.; Chand, K. Effect of slip conditions and hall current on unsteady MHD flow of a viscoelastic fluid past an infinite vertical porous plate through porous medium. *Int. J. Eng. Sci. Technol.* **2011**, *3*, 3124–3133.
34. Li, X.; Faghri, A. Local entropy generation analysis on passive high concentration DMFCs (direct methanol fuel cell) with different cell structures. *Energy* **2011**, *36*, 403–414. [CrossRef]
35. Hayat, T.; Rafiq, M.; Ahmad, B.; Asghar, S. Entropy generation analysis for peristaltic flow of nanoparticles in a rotating frame. *Int. J. Heat Mass Transf.* **2017**, *108*, 1775–1786. [CrossRef]
36. Nouri, D.; Pasandideh-Fard, M.; Oboodi, M.J.; Mahian, O.; Sahin, A.Z. Entropy generation analysis of nanofluid flow over a spherical heat source inside a channel with sudden expansion and contraction. *Int. J. Heat Mass Transf.* **2018**, *116*, 1036–1043. [CrossRef]
37. Dalir, N.; Dehsara, M.; Nourazar, S.S. Entropy analysis for magnetohydrodynamic flow and heat transfer of a Jeffrey nanofluid over a stretching sheet. *Energy* **2015**, *79*, 351–362. [CrossRef]
38. Khan, M.I.; Qayyum, S.; Hayat, T.; Waqas, M.; Khan, M.I.; Alsaedi, A. Entropy generation minimization and binary chemical reaction with Arrhenius activation energy in MHD radiative flow of nanomaterial. *J. Mol. Liq.* **2018**, *259*, 274–283. [CrossRef]

39. Khan, M.I.; Hayat, T.; Waqas, M.; Khan, M.I.; Alsaedi, A. Entropy generation minimization (EGM) in nonlinear mixed convective flow of nanomaterial with Joule heating and slip condition. *J. Mol. Liq.* **2018**, *256*, 108–120. [CrossRef]
40. Hayat, T.; Kanwal, M.; Qayyum, S.; Khan, M.I.; Alsaedi, A. Entropy generation optimisation in the nanofluid flow of a second grade fluid with nonlinear thermal radiation. *Pramana* **2019**, *93*, 54. [CrossRef]